Computational Materials Science 45 (2009) 593–596

Contents lists available at ScienceDirect

Computational Materials Science

journal homepage: www.elsevier.com/locate/commatsci

Numerical study of 3D-compressions of entangled materials

C. Barbier *, R. Dendievel, D. Rodney

SIMAP, Grenoble INP-CNRS-UJF, BP46, 38402 Saint Martin d'Hères, France

ARTICLE INFO

Article history:
Received 29 November 2007
Received in revised form 2 June 2008
Accepted 2 June 2008
Available online 15 July 2008

PACS:
81.05.Lg
61.43.bn
64.60.ah

Keywords:
Computational approach
Semiflexible fibers
Isostatic compression
Coulomb-like static friction

ABSTRACT

We employ a discrete simulation adapted from molecular dynamics techniques in order to study the mechanics of entangled semiflexible fibers. Each fiber is discretized by a small number of segments allowed to stretch and bend. A few hundred fibers, initially straight and placed and oriented at random are simulated during incremental compressions in the three directions of space. Aspect ratios ranging from 20 to 200 were considered. The most important results are (i) an exponent of three is obtained for the pressure–density compression curve, (ii) friction shifts the densities to lower values and (iii) friction does not influence the exponent of the pressure–density curve.

1. Introduction

Entangled materials are made of fibers arranged together in various manners with no permanent cross-link such as sheep wool, glass wool or steel wool …. They exhibit a specific non-linear mechanical behavior which is not fully understood. A first attempt to explain the non-linearity was made by van Wyk [1] who developed a dimensional analysis model for the compression of random fiber networks, based on the statistics of contact formation and on fiber bending between contact points. He found a relationship between the applied pressure (p) and the volume (v):

$$p \propto \left(\frac{1}{v^3} - \frac{1}{v_0^3}\right) \tag{1}$$

where $v = v_0$ when $p = 0$. More refined analytical models were developed including fibers' orientation [2,3], non-overlapping [4,5], crimp [6], large deformations [7] …. But these models did not take into account the fiber rearrangements, i.e. they assume that the contact points move in an affine manner. Refs. [8–10] introduced slippage at contacts, and consequently incremental geometry changes, in order to model realistic energy compression curves and hysteresis during unloading. These works opened the field for the simulation of the compression of entangled materials.

Several authors used Finite Elements methods to perform their studies. Durville [11] used the kinematical beam theory and developed an algorithm to search contacts between fibers to study the loading curve and the number of contacts between fibers during compressions. He obtained results in good agreement with Ref. [7] for large deformations and with van Wyk's model [1] for small deformations. Fibers can also be modeled using Love–Kirchhoff theory as employed by Beil and Roberts [12,13] to study moderate compressions. Their simulations showed a reasonable ability to predict the undetermined constant in van Wyk's equation as well as the hysteresis between compression and unloading curves. These authors were however limited to a small number of fibers and boundary condition effects were not addressed. In all these simulations, friction was taken into account. However, none were interested in the critical density from which there is a mechanical response. A third manner to model fibers is the one used by Rodney et al. [14] on which our work is based. In this method, based on molecular dynamics simulations of polymers, the fibers were discretized by beads in contact with each other. Traction and bending stiffnesses, as well as non-overlapping between fibers, were modeled by means of a potential energy. Isostatic compressions were simulated on initially random fiber configurations in order to study the critical density and the entanglement transition. This method

* Corresponding author. Tel.: +33 4 76 82 63 36; fax: +33 4 76 82 63 82.
E-mail address: carine.barbier@simap.grenoble-inp.fr (C. Barbier).

0927-0256/$ - see front matter © 2008 Elsevier B.V. All rights reserved.
doi:10.1016/j.commatsci.2008.06.003

yielded a stress versus relative density in good agreement with van Wyk's model [1] for large aspect ratios. The main restriction of this model is the fact that the computational load increases rapidly with the fiber aspect ratio that was consequently limited to a value of 100. In this paper, in order to reach larger aspect ratios, we will use a discretization of the fibers in segments to study interactions between fibers during compression. Moreover the influence of static friction at contacts is investigated.

2. Computational model

In this part, we will present the segment model, based on the work of Rodney et al. [14], where the fibers are discretized by a succession of segments of diameter D. This discretization has already been used by Ning and Melrose [15] to study the behavior of isolated fibers in a fluid flow. As proposed in Ref. [14], the behavior of the fiber system is modeled using a potential energy. In the case of the present model, even if the forces are still computed at the nodes (segment ends), the potential energy is now computed from segment lengths and orientations:

$$E = \sum_{i \text{ segments}} \frac{K_S}{2}\left(1-\frac{r_i}{\ell}\right)^2 + \sum_{(i,j) \text{ consecutive}} \frac{K_B}{2}(\theta_{i,j}-\pi)^2 + \sum_{(i,j) \text{ non-consecutive}} \frac{K_I}{2}H(D-r_{i,j})\left(1-\frac{r_{i,j}}{D}\right)^{5/2} \quad (2)$$

The first term corresponds to a linear spring inside each segment. K_S defines the fiber stiffness, ℓ is the initial segment length and r_i its current length. The second term introduces the bending stiffness by means of angular springs between consecutive segments. The angle of π is the equilibrium angle and forces the fibers to be straight when no force is applied. The third term models the contacts between fibers and in particular their non-overlapping. It is a repulsive potential chosen as Hertz potential, that acts between non-consecutive segments when their distance becomes less than the fiber diameter D, which is implied by the Heaviside step function $H(x)$. The distance between segments $r_{i,j}$ is defined as the minimum distance between the two segments i and j (which are assumed straight) computed according to the method of Kumar and Larson [16]. Constants K_S, K_B, K_I are chosen to correspond to those used by Ref. [14]. In particular, K_S was chosen to ensure that the fiber lengths remained close to constant during the simulations. In order to validate this model, the individual fiber behavior is first investigated. First, the resistance of fiber to stretch and compression is directly controlled by K_S: the fiber Young's modulus is $4K_S/\pi D^2\ell$. The bending behavior of a single fiber clamped at one end and subjected to a vertical force F applied to its other end was studied. A good agreement was found between the Finite Element method and the present model both in the linear and non-linear regimes. In particular, in the linear regime, the fiber deflection δ follows a power law well-known in beam theory, $\frac{\delta}{D} = \frac{F}{3}\left(\frac{L}{D}\right)^3\kappa$. The bending stiffness κ can be computed analytically: $\kappa = \frac{D^2}{K_B\ell}\left(1-\frac{\ell}{L}\right)\left(1-\frac{\ell}{2L}\right)$ where ℓ is segment length and L is the fiber length. The buckling of one isolated fiber was also studied. An analytical approach leads for a rod hinged at both ends to a critical force above which the fiber buckles: $F_C = \frac{K_S}{\ell}\left(\frac{1}{2}-\frac{1}{2}\sqrt{1-16\frac{K_B}{K_S}\sin^2\left(\frac{\pi}{2N}\right)}\right)$ where N is the number of segments per fiber. By making the assumption that the number of segments is high, the Euler theory of the critical buckling force is retrieved $F_C \approx \pi^2\frac{K_B\ell}{L^2}$, i.e. the buckling force is inversely proportional to the square of the fiber length. Despite its simplicity, the segment model is able to reproduce three main deformation modes of a fiber: traction, bending and buckling.

Incremental isostatic compressions of fibrous assemblies were simulated. Different systems of homogeneous aspect ratio were considered by placing and orienting fibers initially at random in

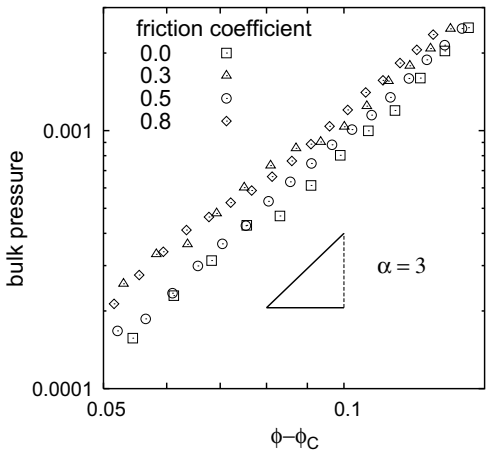

Fig. 2. Log–log plot of the pressure as a function of the difference between the relative density and the packing density for 4-segment fibers of aspect ratio 20 without friction (□), and with friction coefficients equal to 0.3 (△), 0.5 (○), 0.8 (&diam).

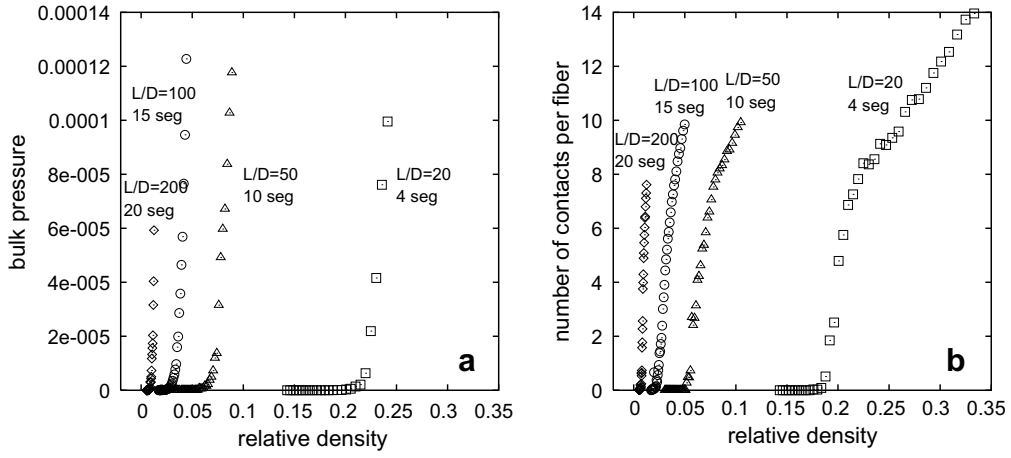

Fig. 1. Bulk pressure (a), and the number of contacts per fiber (b) as a function of relative density 1b for various aspect ratios; □: $L/D = 20$, △: $L/D = 50$, ○: $L/D = 100$, ◇: $L/D = 200$.

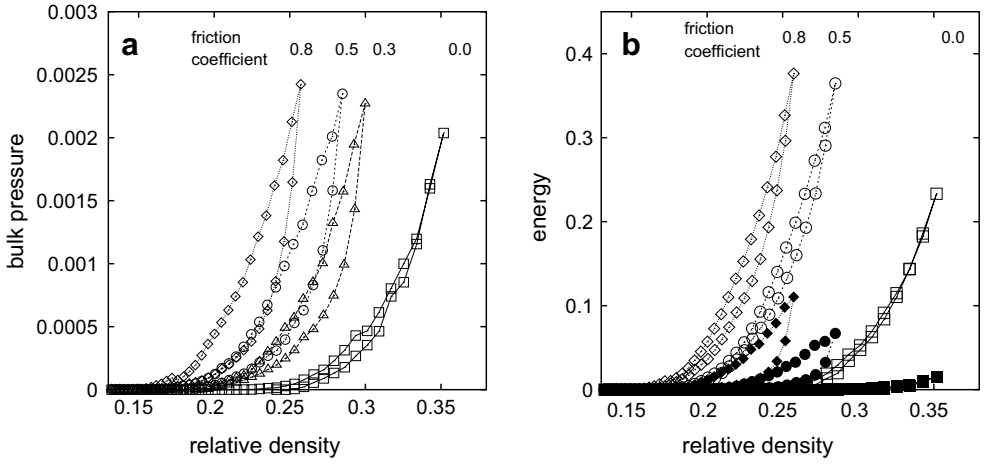

Fig. 3. Pressure (a) and bending (open symbols) and stretching (filled symbols) energies (b) as a function of relative density for 4-segment fibers of aspect ratio 20 without friction (□), and with friction coefficients equal to 0.3 (△), 0.5 (○), 0.8 (◇).

a cubic box. The box size is then decreased incrementally and the fibers are moved homothetically. After each box compression, the system is relaxed to reach equilibrium: the nodal forces are obtained by differentiation of the potential energy (Eq. 2) and the Verlet algorithm [17] is applied on nodes, with the nodal inertial term set to zero whenever the product of the force on a node times its velocity is negative [14]. The number of relaxation steps depends on the segment length: the smaller the length, the larger the number of steps. A number of relaxation steps ranging from 75,000 to 300,000 was used. Fiber arrangements were studied by following up the pressure in the bulk ($P = \frac{1}{3V}\sum_i \mathbf{f}_i \cdot \mathbf{x}_i$ where $\mathbf{x}_i$ the relative position of node i, $\mathbf{f}_i$ the force on node i, V the volume of the box) and the number of contacts per fiber. The number of contacts shown in the following corresponds to the number of contacts supporting a repulsive force not too close to zero which corresponds to a distance between segments lower or equal to $0.9996D$. A Coulomb-like static friction at contact points was also implemented, in order to study the influence of friction between fibers. The friction force is modeled by placing a spring each time a contact is detected between the two contact points on the two fiber surfaces in contact. If the fibers start to slide with respect to each other, the friction spring is stretched, generating a friction force. The spring is maintained until the norm of the friction force becomes greater then the norm of the repulsive force (due to the interaction term in Eq. (2)) multiplied by a friction coefficient (here ranging from 0.0 to 0.8). In such case, the spring is removed and we did not keep track of the sliding contacts. Instead, a new spring is created at the next time step if the contact still exists. A more realistic algorithm, directly adapted from that implemented by Cundall and Strack [18] for spherical granular materials, has also been applied but will not be presented here.

3. Results

Compressions of fibers of different aspect ratios ranging from 20 to 200 were computed. The results shown in Fig. 1a and b are very close to those of Ref. [14]. This shows that the number of nodes per fiber can be reduced (in the range of small deformations) without loss of relevance. In Figs. 1a and b, 4 segments are used to model a fiber of aspect ratio 20, 10 segments for 50, 15 for 100 and 20 for 200. These number of segments represent an optimum between the realism of the simulation and the computational time. It can be seen in Fig. 1a that the pressure is null until a critical density (ϕ_C, the packing density) and then increases non-linearly. Moreover, the number of contacts per fiber (Fig. 1b) goes from zero to a finite number in a small range of relative density around the packing density. This can be understood as a mechanical percolation.

In this condition it not surprising to find a power law relation between the pressure and the relative density $(\phi - \phi_C)^{\alpha}$. The latter is shown in Fig. 2 that presents in a log–log plot the evolution of the pressure as a function of the difference between the actual density and the density at transition. The data without friction are shown as square. They follow a straight line that corresponds to a power-law with an exponent α equal to 3, i.e. the same exponent as appearing in van Wyk relation (Eq. (1)).

The influence of static friction during isostatic compression/release cycles was studied. As shown in Fig. 3, cycles were performed with different amounts of friction (friction coefficient ranging from 0.0 (no friction) to 0.8). The pressure–density plot presented in Fig. 3a shows that when the friction coefficient increases, the packing density decreases. The reason is that friction stabilizes contacts that otherwise would have lead to slippage and fiber rearrangements. A lower density is thus required for the fibers to start to interact. Fig. 3a also shows an hysteresis between the compressions and releases that increases with the amount of friction. Fig. 3b shows that for all amounts of friction, the bending energy is higher than the stretching (the interaction energy is about a tenth of the stretching energy and is not shown here). This is expected because the main deformation mode for these entangled systems is fiber bending around contact points. However, we can also see in Fig. 3b that the role played by stretching increases with friction. Moreover, the hysteresis is more marked on the stretching term than on the bending one. The reason is that frictional contacts resist shear and can lead to fiber stretching. Also, the hysteresis is more marked for the stretching term because the first contacts lost at the beginning of the release are those stabilized by friction which are the ones responsible for fiber stretching. Finally, we can see in Fig. 2 that the exponent α that relates the pressure to the density is not influenced by the friction coefficient. The main effect of friction of the pressure curves is thus to simply shift the curves towards lower densities.

4. Conclusion

This work shows that the number of degrees of freedom of a fiber assembly can be reduced by discretizing the fibers by segments instead of beads without any loss of relevance. Indeed for isostatic compressions, we retrieve the exponent of 3 found by van Wyk [1]. The simulations of compression/unloading cycles

show that hysteresis between compression and unloading increases with friction. Moreover, friction decreases the packing density ϕ_C. One perspective of this work is to perform simulations based on realistic initial configurations. To do this, images of steel wools have been obtained by using 3D X-ray tomography [19]. Our aim is to skeletonize and discretize in segments the X-ray tomography images. We will then be able to perform simulations based on realistic initial configurations extracted from real samples and to compare with the corresponding experimental data.

References

[1] C.M. van Wyk, J. Textile Inst. 37 (1946) T285–T292.
[2] A.E. Stearn, J. Textile Inst. 62 (1971) 353–360.
[3] S. Toll, Polym. Eng. Sci. 38 (1998) 1337–1350.
[4] N. Pan, Textile Res. J. 63 (1993) 336–345.
[5] T. Komori, M. Itoh, Textile Res. J. 64 (1994) 519–528.
[6] T. Komori, M. Itoh, Textile Res. J. 67 (1997) 204–210.
[7] M. Baudequin, G. Ryschenkow, S. Roux, Eur. Phys. J. B 12 (1999) 157–162.
[8] G.A. Carnaby, N. Pan, Textile Res. J. 59 (1989) 275–284.
[9] D.H. Lee, G.A. Carnaby, Textile Res. J. 62 (1992) 185–191.
[10] D.H. Lee, G.A. Carnaby, S. Tandon, Textile Res. J. 62 (1992) 258–265.
[11] D. Durville, J. Mater. Sci. 40 (2005) 5941–5948.
[12] N.B. Beil, W.W. Roberts, Textile Res. J. 72 (2002) 341–351.
[13] N.B. Beil, W.W. Roberts, Textile Res. J. 72 (2002) 375–382.
[14] D. Rodney, M. Fivel, R. Dendievel, Rev. Lett. 95 (2005) 108004.
[15] Z. Ning, J.R. Melrose, J. Chem. Phys. 111 (1999) 10717–10726.
[16] S. Kumar, R.G. Larson, J. Chem. Phys. 114 (2001) 6937–6941.
[17] A. Allen, D. Tildesley, Computer Simulations of Liquids, Oxford University Press, New York, 1987.
[18] P.A. Cundall, O.D.L. Strack, Géotechnique 29 (1979) 47–65.
[19] J.P. Masse, L. Salvo, D. Rodney, Y. Bréchet, O. Bouaziz, Scripta Mater. 54 (2006) 1379–1383.